AGU ADVANCING EARTH AND SPACE SCIENCES

Geophysical Research Letters

RESEARCH LETTER
10.1029/2024GL111269

Special Collection:
Space Weather Events of 2024 May 9-15

Evidence of Unusually Strong Equatorial Ionization Anomaly at Three Local Time Sectors During the Mother's Day Geomagnetic Storm On 10–11 May 2024

Diptiranjan Rout[1], A. Kumar[2,3], R. Singh[4], S. Patra[5], D. K. Karan[6], S. Chakraborty[7], D. Scipion[4], D. Chakrabarty[2], and Juanita Riccobono[8]

[1]National Atmospheric Research Laboratory, Gadanki, India, [2]Physical Research Laboratory, Ahmedabad, India, [3]Laboratorio de Fısica e Astronomia, Universidade do Vale do Paraıba (UNIVAP), Sao Jose Dos Campos, Brazil, [4]Radio Observatorio de Jicamarca, Instituto Geofisico de Peru, Lima, Peru, [5]University of New Brunswick, Fredericton, NB, Canada, [6]Laboratory for Atmospheric and Space Physics, University of Colorado, Boulder, CO, USA, [7]Space and Atmospheric Instrumentation Lab, CSAR, Embry-Riddle Aeronautical University, Daytona Beach, FL, USA, [8]Computational Physics Inc., Lowell, MA, USA

Abstract This study uses multiple ground and satellite-based measurements to investigate the extreme ionospheric response to the Mother's Day storm on May 10–11, 2024. Prompt penetration electric field caused a significant enhancement in the ionospheric vertical drift (∼95 m/s) and the equatorial electrojet strength (∼275 nT) over Jicamarca. These extreme eastward electric field perturbations, along with the large meridional wind, significantly altered the F-region plasma fountain at different local times. The afternoon equatorial ionization anomaly (EIA) not only sustained for an exceptionally long duration (∼12 hr) but also expanded spatially over time. The separation between the two peaks of EIA crests exceeded ∼48° and ∼70° in the morning and evening sectors, respectively. This study shows, for the first time, that unusually strong EIA can not only develop at different local times but can also sustain for long duration under favorable conditions, which has implications for space weather applications.

Plain Language Summary The Earth's upper atmosphere is significantly influenced by space weather events, particularly geomagnetic storms. In this study, we investigate the impact of an intense geomagnetic storm that occurred on 10–11 May 2024 (popularly known as Mother's Day storm) on the equatorial and low-latitude ionosphere. Using datasets from various ground and satellites-based (SWARM, and GOLD satellites, Global GNSS receivers, Incoherent Scatter Radar (ISR), Fabry- Perot interferometers (FPI), and magnetometer) measurements, we show the impact of extreme prompt penetration of electric field on the development of plasma fountain during the storm. We observe a significant increase in electron density and TEC during the main phase of the storm. Our findings highlight the role of extreme space weather disturbances on the generation of EIA at different local times and the impact of the plasma distribution on the globe. We also observe different types of electric field perturbations on low latitude ionosphere during this severe geomagnetic storm.

Key Points:

- The plasma fountain during the Mother's Day storm was unusually strong across different local time sectors
- The combined effects of a strong penetration electric field and meridional wind sustained the plasma fountains for an extended period
- The EIA crest over the Jicamarca sector merged with the expanded auroral region

Correspondence to:
D. Rout,
diptiprl89@gmail.com

Citation:
Rout, D., Kumar, A., Singh, R., Patra, S., Karan, D. K., Chakraborty, S., et al. (2024). Evidence of unusually strong equatorial ionization anomaly at three local time sectors during the mother's day geomagnetic storm on 10–11 May 2024. *Geophysical Research Letters*, *52*, e2024GL111269. https://doi.org/10.1029/2024GL111269

Received 10 JUL 2024
Accepted 14 DEC 2024

1. Introduction

The equatorial ionization anomaly (EIA) is a pivotal feature of the Earth's ionosphere, characterized by two peaks of electron density around ±15° magnetic latitude and a trough near the magnetic equator (Appleton, 1946; Duncan, 1960). This EIA is driven by the interplay between several factors, including ionospheric electric field, neutral winds, tides, magnetic declination, Pre-reversal enhancement (PRE), ion production, and loss rates, resulting in a redistribution of ionospheric plasma (Abdu et al., 1990; Balan et al., 2018; Eastes et al., 2023; Stolle et al., 2008). It is typically observed in the afternoon and evening hours but varies with seasons and geomagnetic activity (Balan et al., 2018; Dias et al., 2020; Kumar et al., 2021; Romero-Hernandez et al., 2018). Geomagnetic storms, primarily induced by solar activities such as coronal mass ejections (CMEs) and high-speed solar wind streams, can inject substantial energy into the Earth's magnetosphere. This energy can lead to pronounced perturbations in the ionosphere, including alterations in the EIA (Appleton, 1946; Balan et al., 2018; Hanson & Moffett, 1966). A few studies have reported the relatively rare early morning EIAs occurring under different geophysical conditions due to varied dynamics (Batista et al., 2006, 2012; Laskar et al., 2020). Prompt penetration electric fields (PPEF) during some geomagnetic storms can cause super-fountains (Balan et al., 2009; Karan

et al., 2024; Mannucci et al., 2005; Rout et al., 2019; Singh et al., 2022; Tsurutani et al., 2008). Understanding the response of the EIA during various space weather conditions is crucial for improving space weather prediction models and mitigating adverse effects on technological systems, including satellite communications, navigation, and radar operations (Balan et al., 2018; Kryukovsky et al., 2021).

Extreme ionospheric conditions were observed during the May 10–12, 2024 Mother's Day storm. In this paper, we present a thorough analysis of the EIA's variations in response to this geomagnetic storm, "the largest in reported Dst in the last two decades," utilizing data from diverse observational platforms. For comparison, Mannucci et al. (2005) reported the super-fountain during the 2003 Halloween storm observed by only GPS TEC measurement over the North American west coast, where the EIA crests were located at ±30° MLat during the afternoon (12:30–13:30 LT). However, for the first time, this study demonstrates that the super-fountain effect can extend beyond ±35° MLat over the Jicamarca meridian and persist for more than 12 hr due to exceptionally large electric fields present during the storm main phase. A rare and strong early morning EIA was also observed at 07:10 LT. The EIA was found to be unusual due to its local time occurrence and latitudinal extension toward higher latitudes. To the best of our knowledge, this is the first report on the variation of the EIA morphology at different local times of an extreme space weather event, which occurred on 10–11 May 2024, using multiple space- and ground-based measurements. This study also shows the different types of electric field perturbations on low latitude ionosphere during this severe geomagnetic storm. Our findings offer valuable insights into the magnetosphere-ionosphere-thermosphere coupling processes and contribute to a broader understanding of ionospheric behavior during extreme space weather events.

2. Observations and Results

2.1. Solar Wind and Geomagnetic Observations

The Interplanetary Coronal mass ejections (ICME), associated with solar flares, erupted from the Sun on 7–9 May 2024 and passed by Earth on 10 May 2024, causing a G5-level super geomagnetic storm. Figure 1 shows the observations of solar wind parameters at the L1 point (in the Geocentric Solar Ecliptic coordinate system) and the strength of the geomagnetic storm quantified by the SYM-H index from 10–12 May 2024. The first ICME hit the magnetosphere at ∼15:00 UT on 10 May 2024, and 2 hours later, at ∼17:00 UT, the Earth's magnetosphere encountered a second stronger ICME. The solar wind parameters (N, V, and P) changed sharply due to the arrival of the interplanetary shocks. The SYM-H index also increased to ∼88 nT due to the rise in P_{dyn} on the arrival of the second Interplanetary (IP) shock. The main phase of the storm started at ∼17:20 UT as the Z-component of interplanetary magnetic field ($IMFB_z$) turned from northward to southward. The geomagnetic storm reached its maximum strength at ∼02:15 UT on May 11 signified by a minimum SYM-H value of −518 nT as IMFBz also attained a minimum value of −52 nT. A few substorms are also observed during both main and recovery phases of the storm as indicated by the AL/AU enhancements.

2.2. Impact on Ionospheric Electric Field: PPEF

The effects of PPEF during this severe geomagnetic storm on the equatorial electric field are investigated based on the vertical plasma drift (Vd_{JIC}) and equatorial electrojet (EEJ) measurements over Jicamarca. Vertical drifts (averaged over 250–450 km altitude) measured by Incoherent Scatter Radar (ISR) over Jicamarca with 5 min temporal resolution are used. The EEJ data with 1 min resolution over the Jicamarca is deduced by subtracting the H-component of the magnetic field measured at an equatorial station to an off-equatorial station, $EEJ_{JIC} = \Delta H_{JIC} — \Delta H_{PIU}$ (Jicamarca (JIC), 11.95° S, 76.87° W, MLat = 0.6° N) and Piura (PIU, 5.2° S, 80.6° W, MLat = 6.9° N) (Anderson et al., 2004).

Figures 1f and 1g show the variations in Vd_{JIC} in m/s along with quiet time model-derived drift from Scherliess and Fejer (1999), and EEJ_{JIC} on event day along with the quiet time variation (averaged over 07–09 May 2024) during 10–12 May 2024. The dashed vertical lines at 17:40 UT, 19:10 UT, and 22:30 UT indicate the onset of substorms during the storm's main phase, with corresponding AL index values of −1,830 nT, −3,797 nT, and −1,989 nT. Significant changes in Vd_{JIC} and EEJ_{JIC} are also noted at these times. One of the striking observations is the huge change in Vd_{JIC} and EEJ_{JIC} at 17:40 UT (12:40 LT), which attained maximum values of ∼95 m/s and ∼275 nT during this event. The EEJ_{JIC} unusually increased over twice the quiet time values on 10 May. It is important to note here that the Vd_{JIC} and EEJ_{JIC} remain mostly positive due to the eastward PPEF on 10 May 2024 after the storm onset, although their magnitude decreases after ∼19:00 UT (14:00 LT) which coincides with the

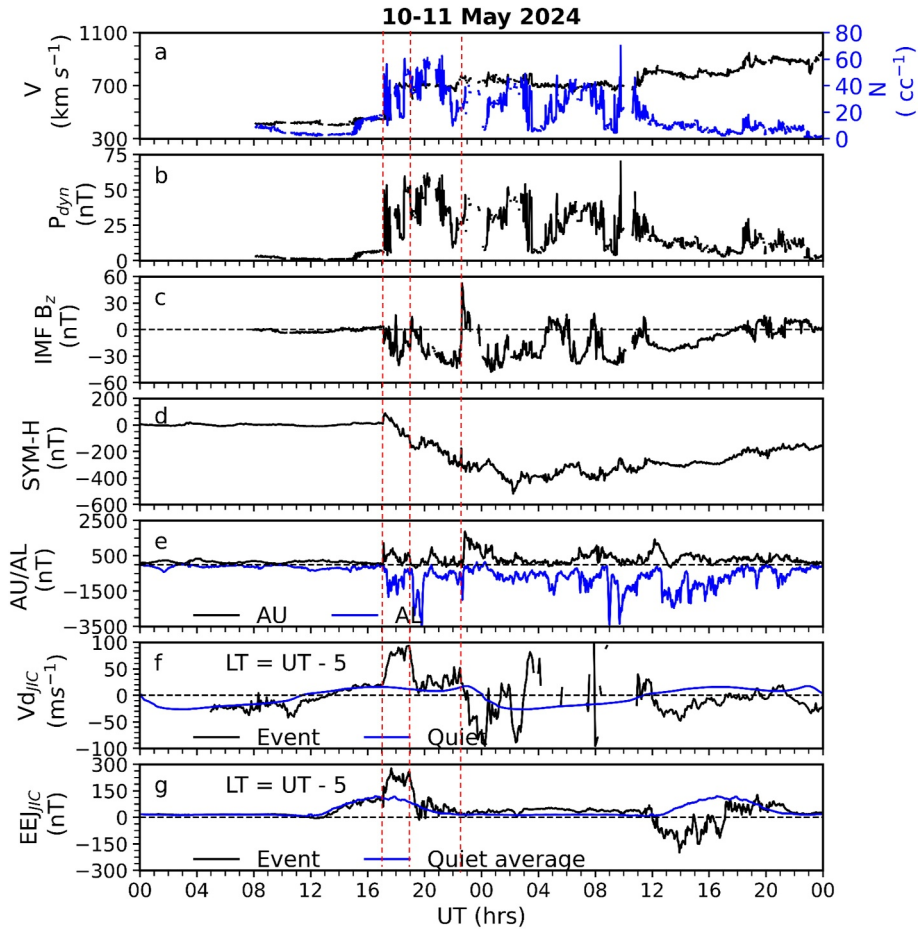

Figure 1. From top to bottom, the panels show, for the event of 2024 May 10–11, variations as a function of time in UT of the following parameters: (a) solar wind velocity (V) and density (N), (b) dynamic pressure (P_{dyn}), (c) IMFBz, (d) SYM-H index, (e) AL/AU indices, (f) Vd_{JIC} along with quiet time drift (in blue line) and (g) EEJ_{JIC} which is overlaid with quiet time average (in blue line). The vertical red dashed-lines are marked to show the onset of substorms during main phase of storm. Local time, LT = UT-5 hrs.

triggering of the second substorm. As the $IMFB_z$ turned northward at ∼22:30 UT (17:30 LT) after being steadily southward, a substorm gets triggered and as a result an overshielding electric field is established. This field was so strong that it not only suppressed the PRE-time eastward electric field (upward drift) but also caused the downward drift to reach a minimum value of about −95 m/s. However, EEJ_{JIC} did not capture this overshielding electric field due to the lower conductivity of the evening-time E-region. Interestingly, EEJ_{JIC} reached ∼-150 nT at 14:00 UT (09:00 LT) on May 11th, indicating a morning counter electrojet, due to the delayed effect of the DDEF which resulted the reduction of thermospheric composition (O/N2) as observed in GOLD measurements (Evans et al., 2024).

2.3. EIA Development During Early Morning and Evening Hours: SWARM Observations

In-situ measurements from SWARM-A satellite that orbits at a height of ∼460 km are used to observe the EIA during morning and evening hours. Figure 2a shows the electron density variations during 09–11 May 2024 as a function of geographic latitude and UT. It is important to note that each satellite passing time of low latitude is marked with universal time and longitude when the satellite is situated at or very close to the geographic equator. Figures 2b and 2c show the latitudinal variations of electron density for quiet (black) and event (red), respectively, for the particular pass. Note that Geographic latitude and Altitude adjusted corrected geomagnetic (AACGM) latitude (now onwards, magnetic latitude (MLat)) are shown on top and bottom *X* axes of Figures 2b and 2c. Figure 2b depicts the evening-time EIA structure for quiet (9th May) and disturbed day (10th May 2024) at 23:11

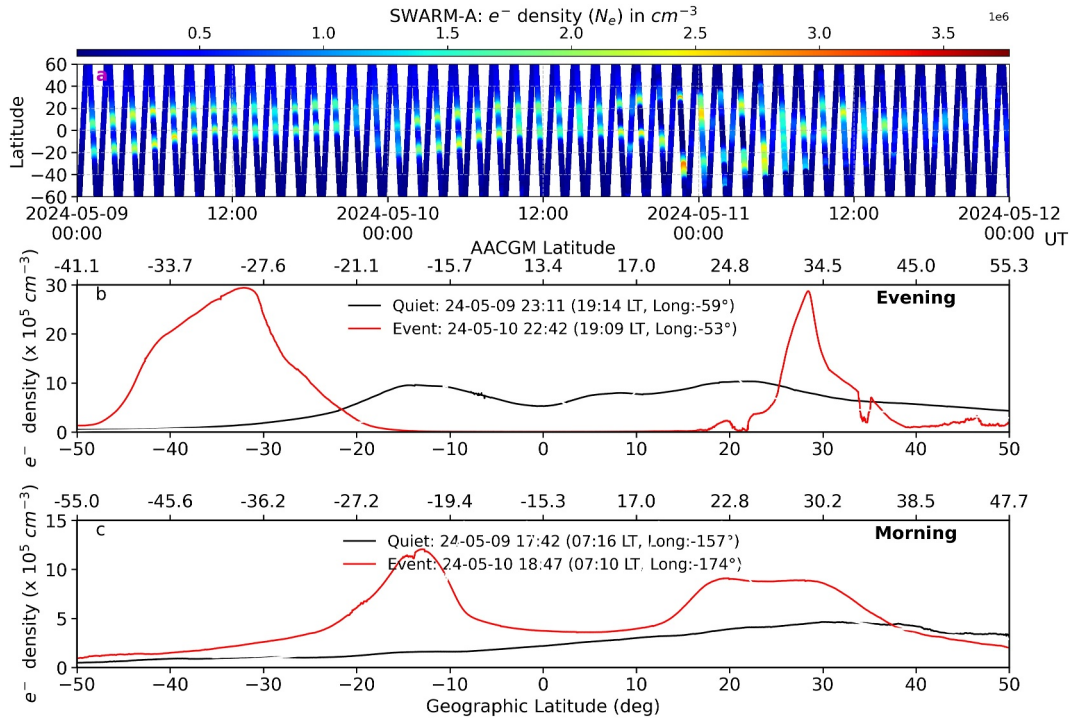

Figure 2. (a) Shows the variation in the electron density during 10–11 May 2024 as a function of UT. (b and c) Shows the electron density variation on the event day (red line) and the previous quiet time (black) with respect to geographic and geomagnetic latitude during the evening and early morning hours, respectively. Each satellite passing time of low latitude is marked with universal time and longitude.

UT (19:14 LT, Geo. Longitude: 59° W) and 22:42 UT (19:09 LT, Geo. Longitude: 53° W) respectively. It can be noticed from Figure 2a that as the storm starts on 10 May, there is a significant increase in the electron density and the latitudinal extent as compared to the previous day. The EIA crests are situated around 15−20° geomagnetic latitudes (MLat) with a peak value of around 10×10^5 cm^{-3} on the previous quiet day (Figure 2b). The scenario changes significantly on the event days. The EIA crests were found to be well separated and located at ∼33.0° MLat in the northern hemisphere and ∼29° MLat in the southern hemisphere during evening local time. This shows that hemispheric asymmetry exists as far as the location of the EIA is concerned, although the peak electron densities remain the same at this time. The peak electron density $\left(\sim 30 \times 10^5 \text{ cm}^{-3}\right)$ of the EIA crests' is more than three times as compared to the previous quiet day.

Figure 2c shows a rare and peculiar morning-time EIA crest observed on 10 May 2024 at 18:47 UT (07:10 LT) along 174° W longitude. For comparison, we considered the quiet pass of SWARM-A on 9 May 2024 at 17:42 UT (07:16 LT) along 157° W longitude, just before the event day. It can be seen that there was no EIA observed on the previous day in the same longitude sector. However, on the event day, a well-developed EIA is evident, with northern and southern crests situated at approximately ∼26.0° and ∼22.0° MLat, respectively, showing a significant increase in electron density. The peak density values of the EIA crests are almost twice or higher compared to the quiet time values although typically no EIA is observed during quiet time. The strength of the morning EIA is exceptionally strong, especially considering its occurrence at 07:10 LT.

2.4. EIA Development During the Afternoon and Evening Hour Over Jicamarca Meridian: GPS-TEC and GOLD Observations

To observe the EIA development at Jicamarca geographic meridian, the GPS-TEC, and GOLD data are presented in Figure 3. Figures 3a and 3b show the maps of GPS TEC and the deviations of TEC (ΔTEC) with universal time crossing Jicamarca during 9–11 May 2024, respectively. Here ΔTEC = (TEC - mean [TEC_{IQDs}]) is the absolute difference of TEC from the five International Quiet Days (IQDs) mean during May. AACGM latitude is calculated at a height of 350 km for GPS TEC. From Figures 3a and 3b, it can be observed that there is a

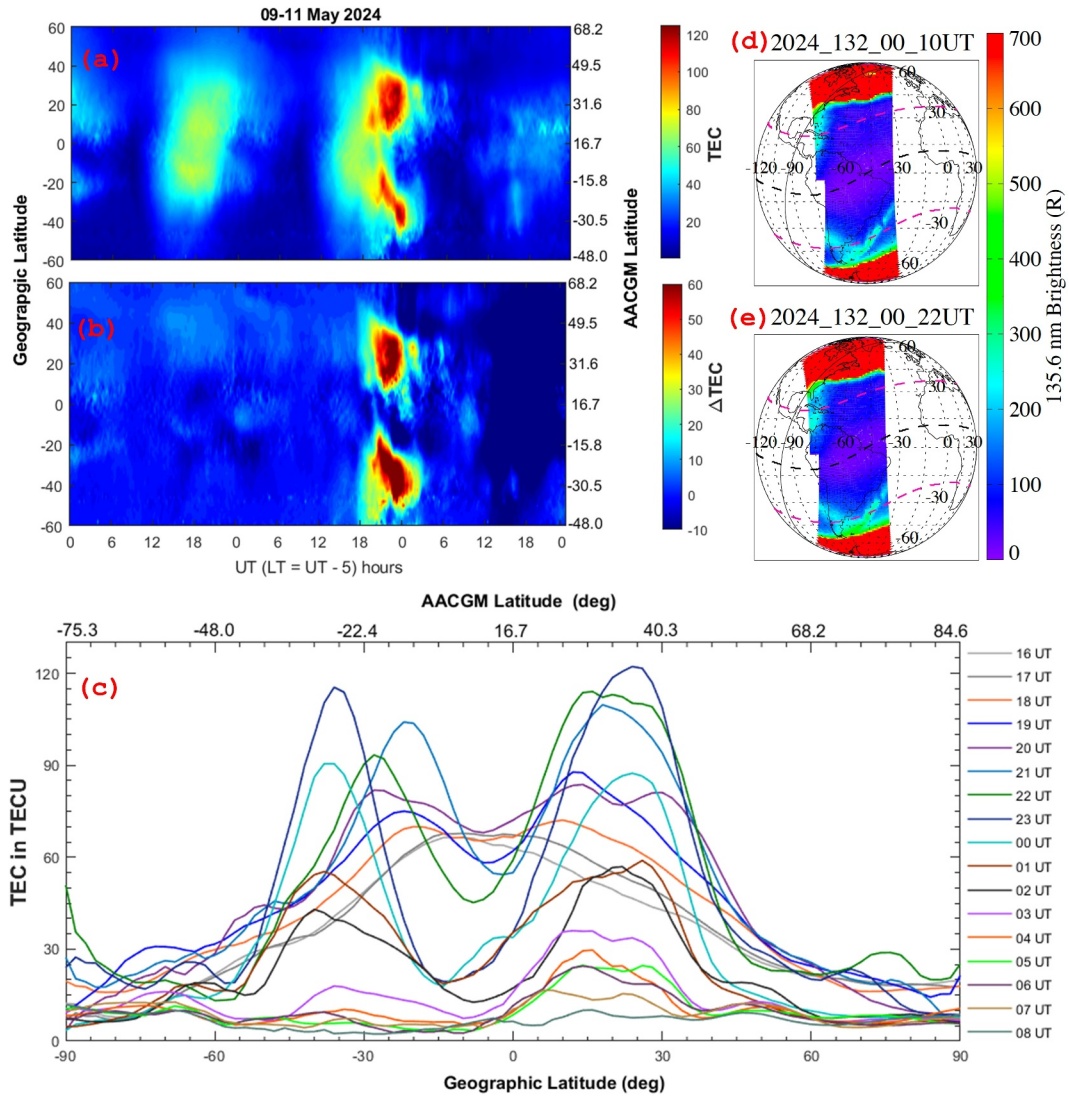

Figure 3. Show (a) the maps of GPS TEC, and (b) ΔTEC = TEC - mean [TEC_{IQDs}], where TEC_{IQDs} is the average value of five IQDs during May with UT over the Jicamarca sector during 9–11 May 2024, respectively. (c) shows the latitudinal variation of hourly TEC values at selected UTs (marked by different colors) on 10–11 May 2024. The geographic and geomagnetic latitudes are also mentioned in the respective figures. (d) and (e) show the GOLD nighttime 135.6 nm images on 11 May 2024 (Day of the Year 132).

significant increase in TEC values on May 10 as compared to the quiet day. The maximum changes in TEC (ΔTEC) values are approximately 380% and 1,300% TECu in the northern and southern hemispheres, respectively, in the crest region. The EIA crests are well-separated and extended to higher latitudes (up to mid-latitudes) due to the continuous eastward PPEF during the storm's main phase (Figure 1). The EIA crests extended from 20°–54° MLat in the northern hemisphere and from 13°–43° MLat in the southern hemisphere. In the recovery phase, EIA crests are significantly suppressed (Figures 3a and 3b) due to the strong westward electric field present on 11 May which is evident from Figures 1f and 1g.

To understand the evolution of the EIA crest after the imposition of the PPEF, we present Figure 3c, which shows the latitudinal variation of hourly TEC values at selected UTs (marked by different colors) on 10–11 May 2024. Initially, the EIA crests were at ± ∼ 15° MLat at 18:00 UT (13:00 LT) similar to the quiet time pattern. Due to the imposition of an extremely large eastward PPEF at 17:40 UT, the EIA crests gradually shifted poleward. By 02:00 UT on 11 May 2024, the EIA crests reached ∼36° MLat in the northern hemisphere and ∼35° MLat in the southern hemisphere along the Jicamarca meridian, clearly demonstrating the formation of a super fountain.

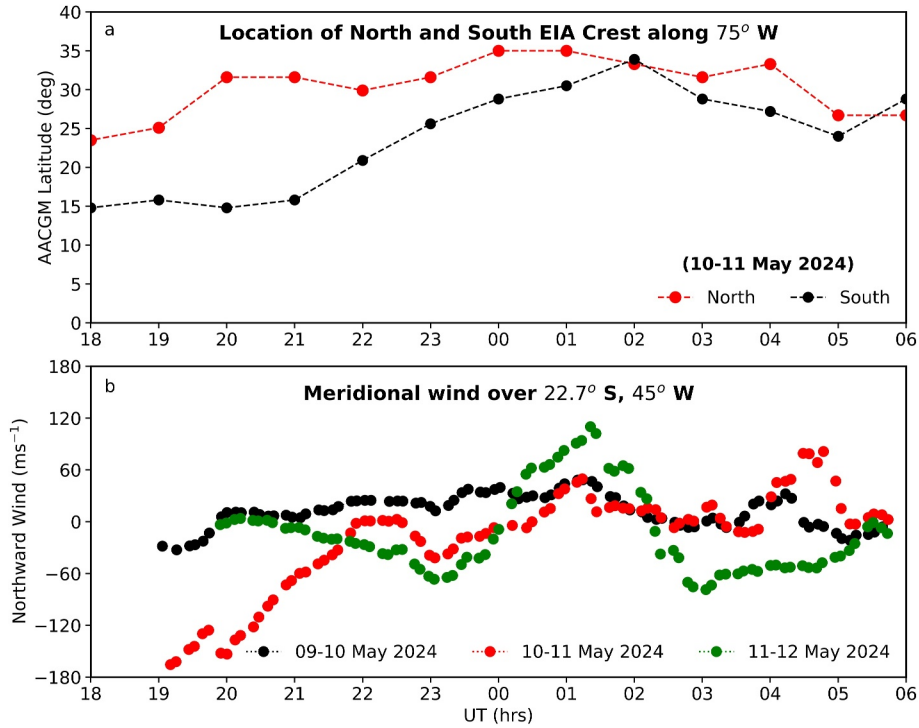

Figure 4. Shows the variation of (a) the EIA crest location derived from GPS TEC in north and south hemisphere along 75° W, during 10–11 May, and (b) the meridional wind over the Brazilian sector (Cachoeira Paulista; 22.7° S, 45° W longitude) on 9, 10, and 11 May 2024.

Notably, the maximum shift of the EIA crest was observed at 02:00 UT on 11 May, although the magnitude of the TEC values decreased. The evolution of the EIA crest appeared to saturate in the northern hemisphere, with no further movement after 20:00 UT, indicating a north-south asymmetry in the formation of the EIA crests. This asymmetry is evident particularly in the latitudinal extent of the crests. It is important to note here that the double peak structure of EIA continued until ∼06:00 UT (01:00 LT) on 11 May which was developed at ∼18:00 UT (13:00 LT) on 10 May, indicating that the EIA not only grew with time but also sustained for a long time (∼12 hr). Panels 3d–3e show NASA's Global-scale Observations of the Limb and Disk (GOLD) observations of OI 135.6 nm emissions at 00:10 and 00:22 UT, respectively, which are only available on the Jicamarca meridian during this event. The EIA crests observed by GOLD at this time are at ∼25° and ∼ − 23° MLat in the northern and southern hemispheres, respectively, whereas the EIA crests observed by TEC are at ∼35° and ∼ − 30° MLat. This indicates that the EIA crests observed by TEC extend more than those observed by GOLD. The nighttime OI 135.6 nm emission, which shows a strong correlation with TEC, primarily results from the radiative recombination of O^+ ions and electrons (Cai et al., 2021; DeMajistre et al., 2004; Rajesh et al., 2011). However, morphological discrepancies, as shown in Figure 3, have also been reported in several studies, especially during geomagnetic storms (Cai et al., 2021; Lei et al., 2015; Maruyama et al., 2004). Additionally, Figures 3d and 3e show that the EIA southern crest even merged with the aurora along ∼60° GLat (Karan et al., 2024).

2.5. Asymmetry in EIA Development and Thermospheric Wind Measurements

Figure 4a shows the EIA crest location (in absolute values of latitudes) derived from GPS TEC in the northern and southern hemispheres along the Jicamarca meridian on 10–11 May 2024. Initially, the separation of the EIA crests (indicating asymmetry) gradually increases, then slowly decreases after 22:00 UT. Notably, the deviation in the northern EIA crest is less (24°–35° MLat), whereas the deviation in the southern crest is more (15°–34° MLat). Figure 4b depicts the wind velocity at a nearby longitude over the Brazilian sector (Cachoeira Paulista (CP); 22.7° S, 45° W; LT = UT-3 hrs). A strong poleward wind (∼-180 m/s) was present in the evening hours on the event day, which was absent on the previous quiet day. Interestingly, the wind speed decreases and closely matches with previous quiet day pattern after 22:00 UT. It seems that as the meridional wind speed weakens the asymmetry in EIA crest location reduces.

3. Discussion

During the main phase of the Mother's Day storm, the ionospheric electric field in the low-latitude region of the American sector was significantly impacted by both eastward and westward fields. The eastward electric field perturbation during day time was driven by PPEF (Fejer & Navarro, 2022; Kelley et al., 2003; Kikuchi et al., 2008), while the westward perturbation during evening hours was caused by the over-shielding of northward turning of IMFBz (Huang, 2020; Kelley et al., 1979) and substorm at 22:30 UT (17:30 LT) (Hashimoto et al., 2017). Notably, during this storm, the sharp increase in P_{dyn} with the arrival of the shock coincides with the change in $IMFB_z$ polarity from northward to southward and also substorm at 17:40 UT (12:40 LT). This suggests that strong eastward PPEF perturbation is associated with changes in P_{dyn} (Huang et al., 2008; Nilam et al., 2023; Rout et al., 2016), $IMFB_z$ and substorm at 17:40 UT (12:40 LT), resulting in significant variations in the equatorial electric field. However, distinguishing the individual effects of these factors remains challenging.

The observation of an early morning EIA at −174° GLon is an important aspect of this storm. Typically, the transition of the quiet-time ionospheric zonal electric field from westward to eastward occurs around 07:00 LT at this longitude (Fejer et al., 2008; Scherliess & Fejer, 1999). For an EIA to develop at this hour, an exceptionally strong eastward electric field is required to reverse the quiet-time polarity. However, due to the lack of additional datasets at this location, it is difficult to ascertain the polarity of the PPEF at this hour. Previous studies using ionosonde measurements over the Brazilian sector have reported similar early morning EIAs during severe geomagnetic storms (Batista et al., 2006, 2012). During this event, a strong early morning (07:10 LT) EIA is detected at −174° GLon by the SWARM-A satellite at an altitude of 460 km. Batista et al. (2012) suggested that large-scale traveling ionospheric disturbances during extreme space weather, along with strong thermospheric meridional winds, are likely responsible for such early morning EIA structures. Additionally, it is noteworthy that the southern EIA crest during evening hours is broader, while the morning EIA exhibits the opposite pattern. This suggests that the direction of the meridional wind is possibly opposite at these two local times. Consequently, a detailed modeling study is crucial to understand the unusual EIA development during the Mother's Day storm.

During the daytime, the latitudinal extension and intensity of EIA crests are primarily controlled by the zonal electric field and ambipolar diffusion leading to a vertical plasma fountain at the magnetic equator, creating enhanced ionization regions $\sim \pm 15°$ away from the equator (Fejer, 1991). In this study, the magnitude of the eastward electric field over the low-latitudes significantly increases as the PPEF is superimposed on the existing quiet-time eastward electric field on at 17:40 UT (12:40 LT) 10 May. Under the influence of the strong eastward electric field, the equatorial F-region plasma is lifted to a higher altitude, causing the EIA crests to shift farther from the geomagnetic equator compared to their quiet time locations. This phenomenon is known as the "dayside ionospheric super fountain effect" (Mannucci et al., 2005; Tsurutani et al., 2008). During the Halloween storm in October 2003, the EIA crests were shifted to $\sim \pm 30°$ MLat (Mannucci et al., 2005) during afternoon hours. However, in this investigation, the EIA crests are formed beyond ±35° MLat in both the hemispheres over the Jicamarca meridian during evening hours. The ionospheric electric field on the event day remained elevated for ∼5 hr compared to the quiet day, although its magnitude decreased after the onset of the substorm at 19:10 UT (14:10 LT) (Figure 1). Due to the sustained eastward electric field on the event day, the ionospheric layer moved upward, reducing the recombination rate and allowing the EIA to persist for a longer duration. Notably, the occurrence of a well-developed EIA crest region during quiet periods can generally be explained by adding a typical diffusion time of 2–3 hr to the time of the maximum eastward electric field over the dip equator around noon (Kumar et al., 2021; Rama Rao et al., 2006). However, this condition may differ during disturbed conditions. In this study, it is evident that EIA can continue for hours under favorable conditions. Further, the modeling study of Balan et al. (2009) suggests that the equatorial plasma fountain rapidly develops into a super fountain due to eastward PPEF in the presence of strong meridional wind. This is evident from Figure 4b that the meridional wind is also significantly high (∼-180 m/s) on the event day as compared to previous day.

To explain most ionospheric processes, particularly during extreme space weather conditions, it is crucial to understand the structure of the thermospheric wind pattern (Bravo et al., 2019). Meridional neutral winds play a crucial role in the development of EIA asymmetry by transporting plasma along magnetic field lines. This transport can lead to variations in the strength, shape, and latitudinal width of the EIA crests, affecting their asymmetry (Khadka et al., 2018; Loutfi et al., 2022). The zonal electric field is also found to be high in this event. Therefore, the influence of meridional wind on the EIA is complex and involves interactions with other factors such as the zonal electric field and geomagnetic activity, which together shape the EIA's asymmetrical

characteristics (Balan et al., 2009; Khadka et al., 2018; Lin et al., 2009; Loutfi et al., 2022). A modeling study is essential to understand the solar wind-magnetosphere-ionosphere-thermosphere coupling processes, shedding light on how such unusual EIAs form at different local times and longitudes during such extreme space weather conditions.

4. Summary

The extreme space weather impact during the Mother's Day storm was investigated using both ground and satellite-based measurements. The key findings from this investigation are.

- The Mother's Day storm of May 10–12, 2023, was stronger than the 2003 Halloween storm, causing significant perturbations in the ionospheric electric field. The combined effect of the extreme PPEF and strong meridional winds drove the unusual EIA over the low-latitude ionosphere at different local times (morning, afternoon, and evening) and also caused the interhemispheric asymmetry in EIA formation. EIA is found to be continued for more than ∼12 hr due to sustained eastward PPEF over the low-latitude ionosphere. The EIA is also found to be extended toward midlatitude and merged with aurora. These factors also caused a significant enhancement in electron density and TEC in the ionosphere, affecting ionospheric plasma distribution.
- ISR and magnetometer measurements over Jicamarca revealed a strong upward drift (∼95 m/s) caused due to change in P_{dyn}, IEFy and substorm during the afternoon hours. Additionally, unusually high downward drift (∼ -95 m/s) was observed due to the overshielding of IEF_y and substorm which suppressed the PRE-time drift. The significantly high westward electric field during the early morning hours over Jicamarca was caused by the disturbance dynamo during the storm's recovery phase.

Data Availability Statement

The solar wind parameters, SYM-H and AL/AU indices are obtained from the OmniWeb service https://cdaweb.gsfc.nasa.gov/. SWARM Satellite data can be downloaded from https://swarm-diss.eo.esa.int/#swarm%2FLevel2daily%2FEntire_mission_data. Magnetometer data over Jicamarca and Piura were obtained from the Low Latitude Ionospheric Sensor Network (LISN) database at http://lisn.igp.gob.pe. ISR-measured drift, GPS TEC, and wind data can be obtained from the Madrigal website (https://www.igp.gob.pe/observatorios/radio-observatorio-jicamarca/madrigal/index.html). The GOLD data are available from the GOLD Science Data Center270 (https://gold.cs.ucf.edu/data/search/).

Acknowledgments

This research is supported by the National Atmospheric Research Laboratory, Department of Space, Government of India. SC thanks the National Science Foundation (NSF) and the National Aeronautics and Space Administration (NASA) for support under grants AGS-1935110 and 80NSSC20K1380, respectively. The Jicamarca Radio Observatory is a facility of the Instituto Geofísico del Perú operated through an agreement with Cornell University, under Prime Agreement AGS-2213849 from the National Science Foundation. A. Kumar extends thanks to the São Paulo Research Foundation (FAPESP) for financial support through Grant 2024/08,104–4. Data production from the Fabry-Perot interferometer at Cachoeira Paulista, Brazil is supported by the Brazilian Ministry of Science, Technology and Innovation, Brazilian Space Agency, CNPq (Grant 311840/2022-1), by NSF award 2431743 and by development funds from Computational Physics Inc. The authors thank Robert Kerr and Jonas Rodrigues de Souza for providing the wind data.

References

Abdu, M. A., Sobral, J., Walker, G., Reddy, B., & Fejer, B. (1990). Electric field versus neutral wind control of the equatorial anomaly under quiet and disturbed condition-a global perspective from sundial 86. *Annales Geophysicae*, *8*, 419–430.

Anderson, D., Anghel, A., Chau, J., & Veliz, O. (2004). Daytime vertical E X B drift velocities inferred from ground-based magnetometer observations at low latitudes. *Space Weather*, *2*(11). https://doi.org/10.1029/2004SW000095

Appleton, E. V. (1946). Two anomalies in the ionosphere. *Nature*, *157*(3995), 691. https://doi.org/10.1038/157691a0

Balan, N., Liu, L., & Le, H. (2018). A brief review of equatorial ionization anomaly and ionospheric irregularities. *Earth and Planetary Physics*, *2*(4), 257–275. https://doi.org/10.26464/epp2018025

Balan, N., Shiokawa, K., Otsuka, Y., Watanabe, S., & Bailey, G. J. (2009). Super plasma fountain and equatorial ionization anomaly during penetration electric field. *Journal of Geophysical Research*, *114*(A3), A03310. https://doi.org/10.1029/2008JA013768

Batista, I., Abdu, M., Nogueira, P. A., Paes, R., de Souza, J., Reinisch, B., & Rios, V. (2012). Early morning enhancement in ionospheric electron density during intense magnetic storms. *Advances in Space Research*, *49*(11), 1544–1552. (Advances in theory and observation of solar system dynamics - I). https://doi.org/10.1016/j.asr.2012.01.006

Batista, I. S., Abdu, M. A., Souza, J. R., Bertoni, F., Matsuoka, M. T., Camargo, P. O., & Bailey, G. J. (2006). Unusual early morning development of the equatorial anomaly in the Brazilian sector during the Halloween magnetic storm. *Journal of Geophysical Research (Space Physics)*, *111*(A5), A05307. https://doi.org/10.1029/2005JA011428

Bravo, M., Batista, I., Souza, J., & Foppiano, A. (2019). Ionospheric response to disturbed winds during the 29 october 2003 geomagnetic storm in the brazilian sector. *Journal of Geophysical Research: Space Physics*, *124*(11), 9405–9419. https://doi.org/10.1029/2019JA027187

Cai, X., Burns, A. G., Wang, W., Qian, L., Liu, J., Solomon, S. C., et al. (2021). Observation of postsunset oi 135.6 nm radiance enhancement over south America by the gold mission. *Journal of Geophysical Research: Space Physics*, *126*(2), e2020JA028108. https://doi.org/10.1029/2020ja028108

DeMajistre, R., Paxton, L., Morrison, D., Yee, J.-H., Goncharenko, L., & Christensen, A. (2004). Retrievals of nighttime electron density from thermosphere ionosphere mesosphere energetics and dynamics (TIMED) mission global ultraviolet imager (GUVI) measurements. *Journal of Geophysical Research*, *109*(A5). https://doi.org/10.1029/2003ja010296

Dias, M. A. L., Fagundes, P. R., Venkatesh, K., Pillat, V. G., Ribeiro, B. A. G., Seemala, G. K., & Arcanjo, M. O. (2020). Daily and monthly variations of the equatorial ionization anomaly (EIA) over the brazilian sector during the descending phase of the solar cycle 24. *Journal of Geophysical Research: Space Physics*, *125*(9), e2020JA027906. https://doi.org/10.1029/2020JA027906

Duncan, R. (1960). The equatorial F-region of the ionosphere. *Journal of Atmospheric and Terrestrial Physics*, *18*(2–3), 89–100. https://doi.org/10.1016/0021-9169(60)90081-7

Eastes, R. W., Karan, D. K., Martinis, C., Daniell, R. E., Gan, Q., Burns, A. G., & McClintock, W. E. (2023). Gold observations of longitudinal variations in the nighttime equatorial ionization anomaly (EIA) crests' latitudes. *Journal of Geophysical Research: Space Physics*, *128*(4), e2022JA031007. https://doi.org/10.1029/2022JA031007

Evans, J. S., Correira, J., Lumpe, J. D., Eastes, R. W., Gan, Q., Laskar, F. I., et al. (2024). GOLD observations of the thermospheric response to the 10-12 may 2024 gannon superstorm. *Geophysical Research Letters*, *51*(16), e2024GL110506. https://doi.org/10.1029/2024GL110506

Fejer, B. G. (1991). Low latitude electrodynamic plasma drifts - a review. *Journal of Atmospheric and Terrestrial Physics*, *53*(8), 677–693. https://doi.org/10.1016/0021-9169(91)90121-M

Fejer, B. G., Jensen, J. W., & Su, S.-Y. (2008). Quiet time equatorial F region vertical plasma drift model derived from ROCSAT-1 observations. *Journal of Geophysical Research*, *113*(A5). https://doi.org/10.1029/2007JA012801

Fejer, B. G., & Navarro, L. A. (2022). First observations of equatorial ionospheric electric fields driven by storm-time rapidly recurrent magnetospheric substorms. *Journal of Geophysical Research: Space Physics*, *127*(12), e2022JA030940. https://doi.org/10.1029/2022JA030940

Hanson, W., & Moffett, R. (1966). Lonization transport effects in the equatorial F region. *Journal of Geophysical Research*, *71*(23), 5559–5572. https://doi.org/10.1029/jz071i023p05559

Hashimoto, K. K., Kikuchi, T., Tomizawa, I., & Nagatsuma, T. (2017). Substorm overshielding electric field at low latitude on the nightside as observed by the HF Doppler sounder and magnetometers. *Journal of Geophysical Research: Space Physics*, *122*(10), 10851–10863. https://doi.org/10.1002/2017JA024329

Huang, C.-S. (2020). Systematical analyses of global ionospheric disturbance current systems caused by multiple processes: Penetration electric fields, solar wind pressure impulses, magnetospheric substorms, and ulf waves. *Journal of Geophysical Research: Space Physics*, *125*(9), e2020JA027942. https://doi.org/10.1029/2020JA027942

Huang, C.-S., Yumoto, K., Abe, S., & Sofko, G. (2008). Low-latitude ionospheric electric and magnetic field disturbances in response to solar wind pressure enhancements. *Journal of Geophysical Research*, *113*(A8). https://doi.org/10.1029/2007JA012940

Karan, D. K., Martinis, C. R., Daniell, R. E., Eastes, R. W., Wang, W., McClintock, W. E., et al. (2024). GOLD observations of the merging of the southern crest of the equatorial ionization anomaly and aurora during the 10 and 11 may 2024 Mother's day super geomagnetic storm. *Geophysical Research Letters*, *51*(15), e2024GL110632. https://doi.org/10.1029/2024GL110632

Kelley, M. C., Fejer, B. G., & Gonzales, C. A. (1979). An explanation for anomalous equatorial ionospheric electric fields associated with a northward turning of the interplanetary magnetic field. *Geophysical Research Letters*, *6*(4), 301–304. https://doi.org/10.1029/GL006i004p00301

Kelley, M. C., Makela, J. J., Chau, J. L., & Nicolls, M. J. (2003). Penetration of the solar wind electric field into the magnetosphere/ionosphere system. *Geophysical Research Letters*, *30*(4), 1158. https://doi.org/10.1029/2002GL016321

Khadka, S. M., Valladares, C. E., Sheehan, R., & Gerrard, A. J. (2018). Effects of electric field and neutral wind on the asymmetry of equatorial ionization anomaly. *Radio Science*, *53*(5), 683–697. https://doi.org/10.1029/2017RS006428

Kikuchi, T., Hashimoto, K. K., & Nozaki, K. (2008). Penetration of magnetospheric electric fields to the equator during a geomagnetic storm. *Journal of Geophysical Research*, *113*(A6). https://doi.org/10.1029/2007JA012628doi:10.1029/2007JA012628

Kryukovsky, A., Lukin, D., Kutuza, B., Bova, Y. I., & Rastyagaev, D. (2021). Study of the effect of the equatorial ionosphere anomaly on the polarizing characteristics of hf radio waves. In *2021 systems of signals generating and processing in the field of on board communications* (pp. 1–7).

Kumar, A., Chakrabarty, D., Pandey, K., Fejer, B. G., Sunda, S., Seemala, G. K., et al. (2021). Evidence for the significant differences in response times of equatorial ionization anomaly crest corresponding to plasma fountains during daytime and post-sunset hours. *Journal of Geophysical Research: Space Physics*, *126*(3), e2020JA028628. https://doi.org/10.1029/2020JA028628

Laskar, F. I., Eastes, R. W., Martinis, C. R., Daniell, R. E., Pedatella, N. M., Burns, A. G., et al. (2020). Early morning equatorial ionization anomaly from gold observations. *Journal of Geophysical Research: Space Physics*, *125*(7), e2019JA027487. https://doi.org/10.1029/2019JA027487

Lei, J., Zhu, Q., Wang, W., Burns, A. G., Zhao, B., Luan, X., et al. (2015). Response of the topside and bottomside ionosphere at low and middle latitudes to the october 2003 superstorms. *Journal of Geophysical Research: Space Physics*, *120*(8), 6974–6986. https://doi.org/10.1002/2015ja021310

Lin, C. H., Richmond, A. D., Bailey, G. J., Liu, J. Y., Lu, G., & Heelis, R. A. (2009). Neutral wind effect in producing a storm time ionospheric additional layer in the equatorial ionization anomaly region. *Journal of Geophysical Research*, *114*(A9). https://doi.org/10.1029/2009JA014050

Loutfi, A., Pitout, F., Bounhir, A., Benkhaldoun, Z., Makela, J. J., Abamni, S., et al. (2022). Interhemispheric asymmetry of the equatorial ionization anomaly (EIA) on the african sector over 3 years (2014–2016): Effects of thermospheric meridional winds. *Journal of Geophysical Research: Space Physics*, *127*(9), e2021JA029902. https://doi.org/10.1029/2021JA029902

Mannucci, A. J., Tsurutani, B. T., Iijima, B. A., Komjathy, A., Saito, A., Gonzalez, W. D., et al. (2005). Dayside global ionospheric response to the major interplanetary events of October 29-30, 2003 "Halloween Storms". *Geophysical Research Letters*, *32*(12), L12S02. https://doi.org/10.1029/2004GL021467

Maruyama, T., Ma, G., & Nakamura, M. (2004). Signature of tec storm on 6 november 2001 derived from dense gps receiver network and ionosonde chain over Japan. *Journal of Geophysical Research*, *109*(A10). https://doi.org/10.1029/2004ja010451

Nilam, B., Tulasi Ram, S., Ankita, M., Oliveira, D. M., & Dimri, A. P. (2023). Equatorial electrojet (EEJ) response to interplanetary (ip) shocks. *Journal of Geophysical Research: Space Physics*, *128*(12), e2023JA032010. https://doi.org/10.1029/2023JA032010

Rajesh, P., Liu, J., Hsu, M., Lin, C., Oyama, K., & Paxton, L. (2011). Ionospheric electron content and NmF2 from nighttime OI 135.6 nm intensity. *Journal of Geophysical Research*, *116*(A2). https://doi.org/10.1029/2010ja015686

Rama Rao, P. V. S., Gopi Krishna, S., Niranjan, K., & Prasad, D. S. V. V. D. (2006). Temporal and spatial variations in TEC using simultaneous measurements from the Indian GPS network of receivers during the low solar activity period of 2004-2005. *Annales Geophysicae*, *24*(12), 3279–3292. https://doi.org/10.5194/angeo-24-3279-2006

Romero-Hernandez, E., Denardini, C. M., Takahashi, H., Gonzalez-Esparza, J. A., Nogueira, P. A. B., de Pádua, M. B., et al. (2018). Daytime ionospheric tec weather study over Latin america. *Journal of Geophysical Research: Space Physics*, *123*(12), 10345–10357. https://doi.org/10.1029/2018JA025943

Rout, D., Chakrabarty, D., Sekar, R., Reeves, G. D., Ruohoniemi, J. M., Pant, T. K., et al. (2016). An evidence for prompt electric field disturbance driven by changes in the solar wind density under northward imf bz condition. *Journal of Geophysical Research: Space Physics*, *121*(5), 4800–4810. https://doi.org/10.1002/2016JA022475

Rout, D., Pandey, K., Chakrabarty, D., Sekar, R., & Lu, X. (2019). Significant electric field perturbations in low latitude ionosphere due to the passage of two consecutive icmes during 6–8 september 2017. *Journal of Geophysical Research: Space Physics*, *124*(11), 9494–9510. https://doi.org/10.1029/2019JA027133

Scherliess, L., & Fejer, B. G. (1999). Radar and satellite global equatorial F region vertical drift model. *Journal of Geophysical Research*, *104*(A4), 6829–6842. https://doi.org/10.1029/1999JA900025

Singh, R., Lee, Y. S., Song, S. M., Kim, Y. H., Yun, J. Y., Sripathi, S., & Rajesh, B. (2022). Ionospheric density oscillations associated with recurrent prompt penetration electric fields during the space weather event of 4 november 2021 over the east-asian sector. *Journal of Geophysical Research: Space Physics*, *127*(6), e2022JA030456. https://doi.org/10.1029/2022JA030456

Stolle, C., Manoj, C., Lühr, H., Maus, S., & Alken, P. (2008). Estimating the daytime equatorial ionization anomaly strength from electric field proxies. *Journal of Geophysical Research*, *113*(A9). https://doi.org/10.1029/2007ja012781

Tsurutani, B. T., Verkhoglyadova, O. P., Mannucci, A. J., Saito, A., Araki, T., Yumoto, K., et al. (2008). Prompt penetration electric fields (PPEFs) and their ionospheric effects during the great magnetic storm of 30-31 October 2003. *Journal of Geophysical Research*, *113*(A5), A05311. https://doi.org/10.1029/2007JA012879